

# Computer-Aided Diagnostics and Pattern Recognition: Automated Glaucoma Detection

9

Thomas Köhler, Rüdiger Bock, Joachim Hornegger,  
and Georg Michelson

## Contents

9.1	<b>Introduction</b> .....	93
9.2	<b>Imaging Modalities</b> .....	94
9.3	<b>Excursus: Pattern Recognition Pipeline</b> .....	95
9.4	<b>Glaucoma Detection by Means of Imaging</b> .....	97
9.4.1	Structure-Driven Glaucoma Detection .....	97
9.4.2	Data-Driven Glaucoma Detection .....	99
9.5	<b>Summary</b> .....	100
9.5.1	Performance Comparison .....	100
9.5.2	Structure-Driven vs. Data-Driven Approach .....	102
	<b>Conclusion</b> .....	102
	<b>References</b> .....	102

T. Köhler, MSc (✉) • R. Bock  
J. Hornegger, Dr.-Ing.  
Pattern Recognition Lab, Department of  
Computer Science, Friedrich-Alexander-Universität  
Erlangen-Nürnberg, Erlangen, Bavaria, Germany

Erlangen Graduate School in Advanced Optical  
Technologies (SAOT), Erlangen, Bavaria, Germany  
e-mail: [thomas.koehler@fau.de](mailto:thomas.koehler@fau.de)

G. Michelson, MD  
Friedrich-Alexander-Universität Erlangen-Nürnberg,  
Erlangen Graduate School in Advanced Optical  
Technologies (SAOT), Erlangen, Bavaria, Germany

Department of Ophthalmology, Interdisciplinary  
Center of Ophthalmic Preventive Medicine and  
Imaging, Friedrich-Alexander-Universität Erlangen-  
Nürnberg, Erlangen, Bavaria, Germany

## 9.1 Introduction

Glaucoma is a retinal disease influencing the *optic nerve head* (ONH) by damaging ganglion cells. Today, it is the second leading cause of blindness worldwide, affecting more than 60 million people in 2010. This number is estimated to increase to about 80 million in 2020 [1]. In the USA, more than 2.2 million people suffer from glaucoma, accounting for more than 9 % of all cases of blindness. In terms of economic impacts, this causes more than ten million physician visits and expenses of about US\$1.5 billion per year [2].

The untreated glaucoma disease causes a successive degeneration of retinal nerve fibers particularly in the ONH region that leads to progressive narrowing of the visual field up to complete blindness. Proper treatment can stop the progress although already degenerated nerve fibers cannot be reactivated. Thus, the early detection and treatment of the disease are essential.

The initial diagnosis of glaucoma [3, 4] is extensive and consists of the assessment of:

1. Risk factors such as high intraocular pressure, race, age etc.
2. The front chamber angle
3. The morphology of the ONH (Sect. 9.4.1)
4. Possible defects of the visual field

Furthermore, a longitudinal assessment of the ONH is performed to confirm the initial diagnosis. Despite the steady rise of diseases over the past years, glaucoma is often undiagnosed until the unrecoverable structural damage of retinal nerve

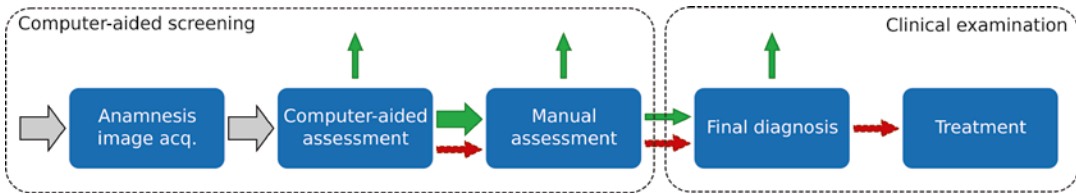


**Fig. 9.1** Computer-aided screening consists of subsequent building blocks: Initially, the anamnesis and image data of the entire screening collective is analyzed to preselect unsuspecting cases. The remaining set has to be

manually assessed for further exclusion of unremarkable subjects. Only a small proportion of the initial set will be forwarded to clinical assessment to gain a final diagnosis and follow-up treatment if necessary

fibers gets evident by the significant narrowing of the visual field. Several studies showed that screening programs for glaucoma [5] can reduce this high number of unreported cases. The main goal of these screening applications is the detection of suspicious cases from a large population and their successful routing to more extensive clinical examination for a final diagnosis. Common screening populations are characterized by a high amount of normals which have to be assessed manually by the involved reading center (Fig. 9.1 step (3)).

*Computer-aided diagnostics* (CAD) supports an ophthalmologist in the preparation of a medical diagnosis based on automatic data-mining methods. In particular, CAD is applicable in screening setups in order to reduce the number of normals for manual judgment, which helps to increase the efficiency of the reading centers (Fig. 9.1 step (2)). This is done by an upstream analysis of the personal data, e.g. images or anamnesis data, utilizing pattern recognition techniques that automatically perform a preselection of suspicious cases. Here, a computer-aided assessment augments the manual assessment provided by the reading center. As depicted in Fig. 9.1, this approach is considered as *computer-aided screening* (CAS). The proposed strategy can also be realized in a telemedical setup where image acquisition and examination are done spatially and temporally separated.

### Scope

This contribution provides an overview on the recent advances in the development of pattern recognition techniques for automatic glaucoma detection. We will focus on fully automatic techniques applicable within a screening environment utilizing pure structural retinal fundus data published in 2008 or later.

### Outline

The remainder of this chapter is organized as follows: After the introduction of common imaging modalities to document ONH morphology, we provide an excursus on pattern recognition. As major part of this work, two methodologies are presented that arise from current automatic glaucoma detection literature on structural retinal image data: (i) structure-driven and (ii) data-driven techniques. Finally, the methods are compared and evaluated toward the application in CAS.

## 9.2 Imaging Modalities

One main part in diagnosing glaucoma is the assessment of the ONH morphology. Besides the slit lamp that allows a live examination of the eye background, several digital imaging modalities got established. These devices allow the documentation of the ONH's structure by acquiring 2-dimensional (2-D) or 3-dimensional (3-D) image data as shown in Fig. 9.2.

*Fundus imaging* is one of the most commonly used technologies in ophthalmology to obtain high-resolution color photographs of the human retina [7, 8]. The fast image acquisition and relatively low costs of a digital fundus camera make this modality attractive to document the retina during screening. The acquired images can be analyzed to detect pathological degenerations caused, e.g., by glaucoma [9].

*Confocal laser ophthalmoscope* commercially available as *Heidelberg retina tomograph* (HRT) [10] acquires topographic and gray-scaled reflectance images of the ONH. In particular, the topographic images capturing the ONH's shape allow the extraction of parameters to discriminate between normals and glaucomatous subjects [11].

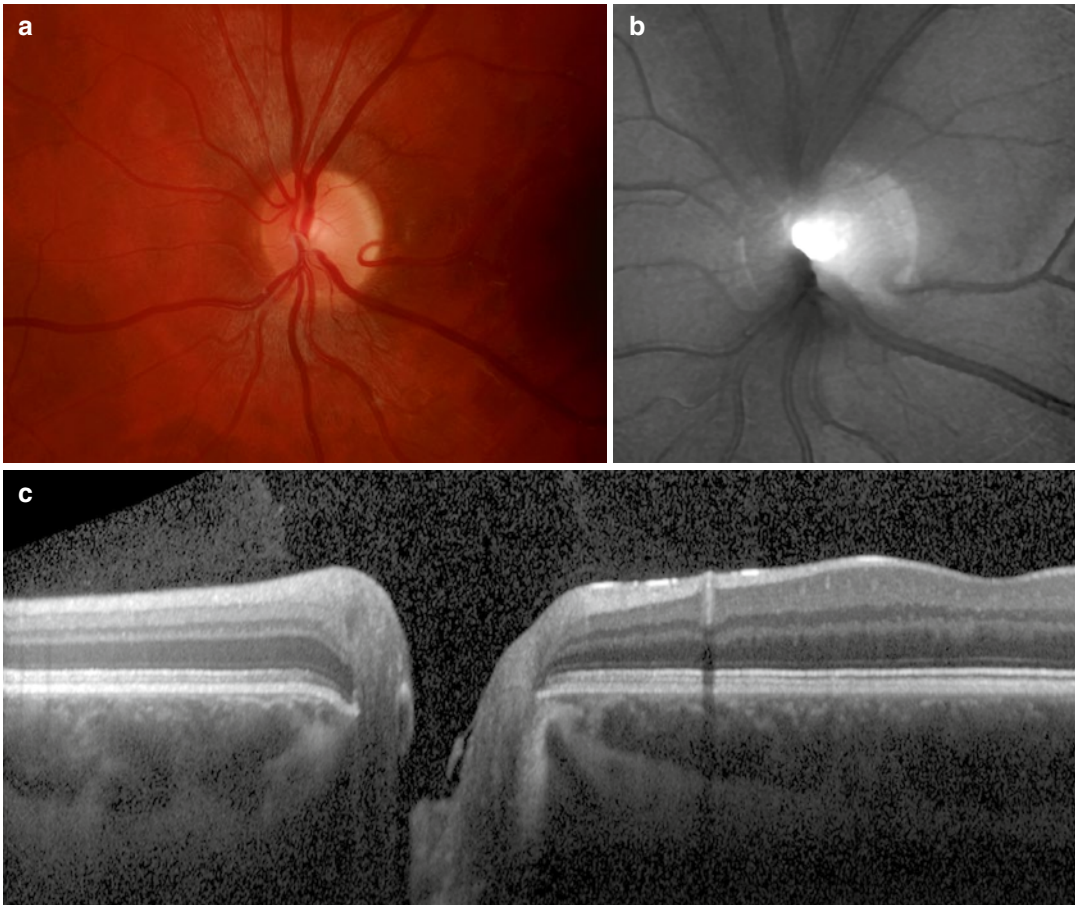


**Fig. 9.2** Sample images capturing the optic nerve head (ONH) region: (a) high-resolution color fundus image, (b) topographic image acquired with Heidelberg retina tomograph (HRT), and (c) OCT line scan intersecting the ONH

and depicting the different retinal layers including the retinal nerve fiber layer as the top one (Reprinted from [6] with permission from Elsevier)

*Optical coherence tomography (OCT)* [12] as the optical pendant to ultrasound enables the acquisition of depth profiles and even entire 3-D volumes of the retina. As the image data also records the *retinal nerve fiber layer* (RNFL), OCT data allows a detailed judgment of the retinal constitution and a reliable diagnosis of glaucoma. In addition, OCT data can be utilized for CAD applications as it was demonstrated by Huang and Chen [13] and Burgansky et al. [14]. As an alternative device for measuring the RNFL thickness, also scanning laser polarimetry (SLP) can be utilized.

From this retinal image data, pattern recognition techniques can extract glaucoma-related markers utilized during the computer-aided assessment within a screening scenario as shown in Fig. 9.1.

### 9.3 Excursus: Pattern Recognition Pipeline

The goal of pattern recognition is to analyze and classify patterns such as images or speech. For this purpose, pattern recognition systems are divided into multiple processing stages that are organized as a pipeline with similar underlying structure for different real-world problems [15]. In terms of glaucoma detection based on retinal image data, this pipeline is outlined in Fig. 9.3. Please also refer to Fig. 9.1 as the pattern recognition pipeline can be embedded within the automated glaucoma assessment step.

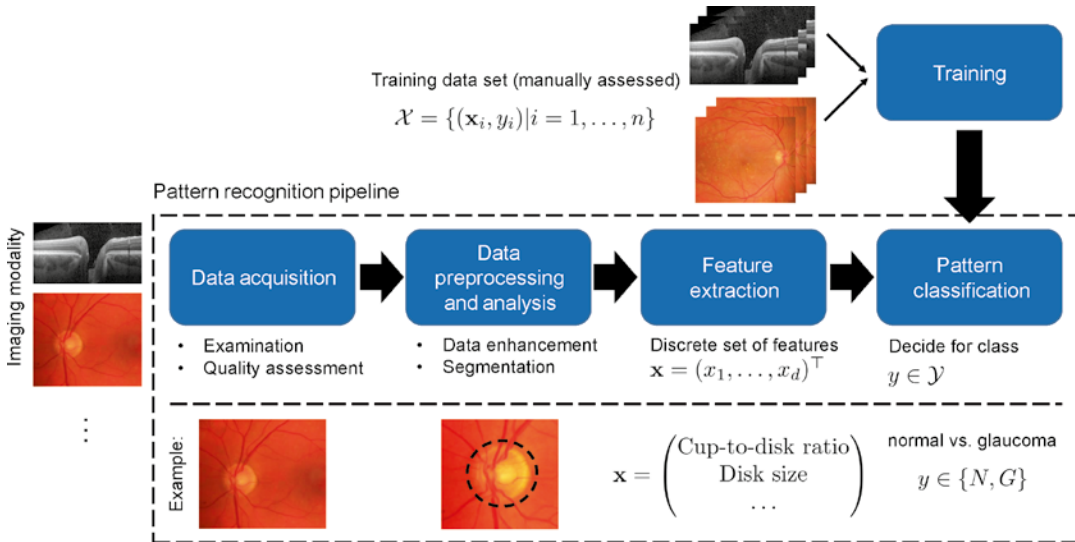


**Fig. 9.3** Pattern recognition pipeline applied to automated glaucoma detection: Retinal image data is (i) acquired with an eye imaging modality such as fundus imaging or optical coherence tomography (OCT), (ii) preprocessed and analyzed as preparation for pattern recognition

techniques, (iii) used to extract relevant features to detect traces of glaucoma, and (iv) used in a classification stage trained with manually classified image data. A common example workflow is visualized for glaucoma detection based on fundus photographs

### Data Acquisition

In an initial data acquisition stage, sensor data such as images or speech is captured. Analog sensor data is commonly converted into a *discrete* mathematical representation for further processing by means of pattern recognition methods.

*Example:* For image-based glaucoma detection, the human eye is captured with an imaging modality. In a common clinical workflow, digital fundus cameras are employed to analyze the optic nerve for traces of glaucoma. As glaucoma detection relies on the quality of the acquired image, data acquisition also involves quality assessment for image data. In case of fundus imaging, several automatic and objective quality indices have been proposed to recognize images not usable for further processing [16–18].

### Data Preprocessing and Analysis

Pattern recognition techniques require an appropriate preparation of the acquired data. Therefore, preprocessing steps are required to correct invalid or erroneous measurements present in the raw data. Different parts of the acquired signal that are relevant for a specific pattern recognition

problem are extracted and analyzed. Then, these parts are used to measure certain parameters and to classify patterns in the underlying sensor data.

*Example:* Retinal image analysis [19] provides methods to process and analyze retinal image data in order to measure clinical parameters of the eye. In terms of fundus imaging, preprocessing for image enhancement includes illumination correction [20] to adjust uneven contrast and denoising techniques [21] to enhance the quality of noisy data. Preprocessing is also beneficial to remove features not related to glaucoma and to make the measurement of disease-specific parameters more reliable [22]. Common analysis steps include a segmentation of the ONH for glaucoma assessment [23–25].

### Feature Extraction

Feature extraction reduces the complexity of the prepared data by modeling it with a finite set of features organized as a *feature vector*  $\mathbf{x} \in \mathbb{R}^d$ . Each single feature  $x_i$  is a mathematical description of a certain parameter or measurement. Features can be either continuous, e.g., geometric measurements such as lengths or diameters of

anatomical structures, or discrete, e.g., the sex of a human subject. Additionally, dimensionality reduction may be used in an optional step to reduce the complexity of raw features  $\mathbf{x}$  to obtain a compressed feature vector  $\mathbf{x}' \in \mathbb{R}^{d'}$  where  $d' < d$ . Feature selection techniques learn the most meaningful features  $\mathbf{x}'$  in an automatic manner based on example data. Opposed to this approach, *principal component analysis* (PCA) is a common tool to perform dimensionality reduction in an unsupervised procedure.

*Example:* Features that can be extracted from fundus images are geometric parameters of the ONH segmented in the previous stage of the pipeline. This includes the well-known *cup-to-disk ratio* (CDR) denoted as  $x_1$  or the size of the optic disk denoted as  $x_2$ . The associated feature vector is given by  $\mathbf{x} = (x_1, x_2)^T$ .

#### Pattern Classification

Sensor data represented by a feature vector  $\mathbf{x}$  is characterized by a *class label*  $y \in \mathcal{Y}$  where  $\mathcal{Y} = \{y_1, \dots, y_k\}$  denotes a discrete set of  $k$  classes. However, the true class label is unknown and must be determined from the features. A *classifier* predicts a class label  $y^*$  from the features  $\mathbf{x}$  in an automatic manner. Therefore, the classifier is derived from a *training set*  $\mathcal{X} = \{(\mathbf{x}_i, y_i) \mid i = 1, \dots, n\}$  to learn the relationship between the features  $\mathbf{x}_i$  and the associated class  $y_i$ . The set  $\mathcal{X}$  is composed from  $n$  training patterns  $\mathbf{x}_1, \dots, \mathbf{x}_n$ , where the true class label  $y_i$  for each  $\mathbf{x}_i$  is known and is used as gold standard. State-of-the-art classifiers commonly used in practical applications are support vector machines (SVM), random forests, artificial neural networks (ANN), or boosting methods such as AdaBoost [15].

*Example:* In glaucoma detection, we are interested in the state of glaucoma, and the aim is to solve a two-class problem with  $y \in \{N, G\}$  whereas  $y = N$  for a normal subject and  $y = G$  for a subject suffering from glaucoma, respectively. Nayak et al. [9] proposed an ANN to discriminate between healthy normals and glaucomatous eyes based on features gained from fundus images. Therefore, the ANN is trained with patterns obtained from manually labeled fundus images provided by an ophthalmologist.

## 9.4 Glaucoma Detection by Means of Imaging

One trend in ophthalmology is the quantitative survey of the retinal fundus based on image data acquired in a noninvasive and in vivo way. These techniques utilize characteristics of the ONH as parameter and can be embedded within glaucoma screening programs [26]. As already depicted in Sect. 9.1, they can be automatically employed within a computer-aided assessment step to detect traces of glaucoma based on image data and to provide an initial exclusion of most likely normal cases.

Two major types of methodologies can be distinguished:

*Structure-driven* techniques commonly automate the extraction of established structural parameters of the ONH, e.g., the diameters of the optic disk and cup. These parameters are already known in the medical community and also statistically verified but are often determined manually.

*Data-driven* techniques utilize data-mining methods applied on the *entire* image to obtain discriminative markers for glaucoma detection. In contrast to structure-driven techniques, no direct relation between the ONH structure and the marker can be further obtained.

### 9.4.1 Structure-Driven Glaucoma Detection

In structure-driven glaucoma detection, disease-specific indicators of clinical significance are measured quantitatively. In general, glaucoma is characterized by a continuous, irreversible loss of ganglion cells [3]. This loss is the root cause for a set of structural ONH changes which can be captured by fundus imaging modalities as introduced in Sect. 9.2: (i) Thinning of the neuroretinal rim and (ii) a simultaneous extension of ONH cupping can be measured in fundus photographs and HRT images [27] as shown in Fig. 9.4 for an example fundus image [8]. (iii) The thinning of the retinal nerve fiber layer can be quantified, e.g., by OCT devices, and correlates with visual field defects due to glaucoma [28].

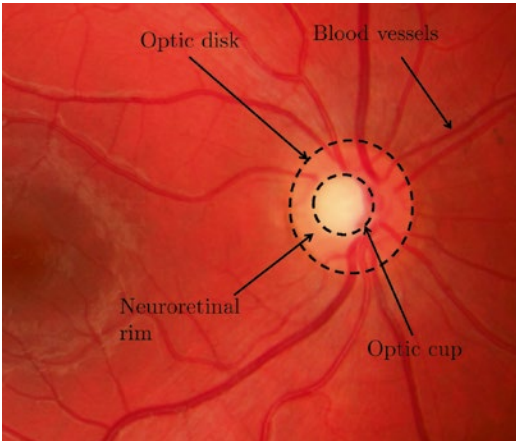


**Fig. 9.4** Fundus image showing the optic nerve head (ONH): The optic cup is visible as bright spot inside the optic disk enclosed by the neuroretinal rim (Image data is taken from the high-resolution fundus (HRF) database)

#### 9.4.1.1 2-D Optic Nerve Head Analysis

A medically established feature accepted for glaucoma diagnosis is the *cup-to-disk ratio* (CDR) defined as:

$$CDR = \frac{d_{cup}}{d_{disk}} \quad (9.1)$$

where  $d_{cup}$  and  $d_{disk}$  denote the vertical cup and disk diameter, respectively. With a thinned neuroretinal rim and an enlarged cup in case of glaucomatous eyes, a larger CDR indicates an increased risk of glaucoma.

Originally, the CDR was manually determined. An automated calculation is possible when utilizing recent image segmentation algorithms. A supervised procedure employs pixel classification to discriminate between disk, cup, and remaining background, e.g., based on superpixels [25]. Contrary, region-based methods rely on active contour models for disk segmentation and vessel-bend detection [23]. In case of stereo fundus imaging, the depth map obtained from a stereo image pair can be utilized to increase the reliability of the cup segmentation [29]. Once disk and cup are segmented,  $d_{cup}$  and  $d_{disk}$  are measured to determine the CDR according to Eq. (9.1).

The CDR may also be combined with further structural features such as the blood vessel areas

in *inferior, superior, nasal, and temporal* (ISNT) quadrants or the distance between optic disk center and ONH as proposed by Nayak et al. [9]. The optic disk size should also be included to glaucoma classification as it highly correlates with CDR [30].

#### 9.4.1.2 Topographic Optic Nerve Head Analysis

One inherent limitation of the CDR is that it ignores the underlying surface of the ONH as it is a 2-D feature only. HRT imaging enables the topographic analysis of the optic nerve which has been also investigated for glaucoma detection [11, 31].

In the approach of Swindale et al. [11], a surface model  $z: \mathbb{R}^2 \rightarrow \mathbb{R}$  estimated from ONH images defines the depth  $z$  as a function of the position  $(u, v)$  on the ONH. This model consists of two parts modeling the surface: (i) the parabolic retinal fundus and (ii) the ONH cup, which is parameterized by ten features. These encode meaningful structural features such as center, radius, slope, or depth of the optic cup as well as secondary parameters such as cup gradient measures derived from the model. They differ for healthy and glaucomatous subjects and are utilized for glaucoma detection. The resulting *glaucoma probability score* (GPS) is obtained by a Bayes classifier which allows to introduce an adapted *loss functions* [15] in order to penalize a misclassification of a glaucoma patient as a healthy one, usually referred to as false negative. This is useful in a screening scenario where unrecognized cases should be avoided.

Twa et al. [32] modeled the ONH depth profile utilizing pseudo-Zernike radial polynomials. The parameters are then used as features within a decision tree classification. This method can be considered as a generalization of Swindale et al. [11] as a generic parametric function is used in comparison to a cup-specific parametric model.

#### 9.4.1.3 Volumetric Retinal Nerve Fiber Layer Analysis

In addition to 2-D and topographic modalities, OCT imaging enables an in-depth analysis of the retinal layers. To enable a reliable determination

of the RNFL, modality-specific image artifacts such as speckle noise [33–35] and motion artifacts [36] need to be compensated beforehand. Afterward, an automatic analysis of the RNFL by image processing and classification methods is promising for glaucoma detection [13, 14].

A threshold-based classification schema considering the single average RNFL thickness is proposed by Pachiyappan et al. [37]. The RNFL is automatically segmented by active contours.

The amount of input features is extended by Bizios et al. [38] who added new parameters to the conventional structural measurements that capture percentile thickness values of different retinal quadrants around the ONH. For classification, (i) an SVM and (ii) neural network classifiers were applied and compared.

An automatic framework for glaucoma detection that also extends the feature space has been proposed by Mayer et al. [39]. Based on an automatic segmentation of the RNFL in *circular B-scans* centered at the ONH [40], the following features are extracted from the RNFL thickness profile and used as classifier input: (i) statistical features including minimum, maximum, and mean values of the profile and (ii) the entire thickness profile compressed by a PCA model. The yielded feature vector  $\mathbf{x}$  only represents the appearance of the RNFL without including any anamnesis data and is utilized by an SVM classifier.

Overall, the structure-driven methods for glaucoma detection mainly rely on a small set of highly discriminative and medically motivated features.

## 9.4.2 Data-Driven Glaucoma Detection

In data-driven approaches, the *entire* image data is exploited by general-purpose features such as spectral or texture features that are established in signal and image processing. These features are neither directly related to glaucoma nor of clinical meaningfulness but represent an abstract mathematical description of the retina. Novel techniques employing this concept for glaucoma detection are described in the following sections.

### 9.4.2.1 Higher-Order Spectra (HOS) and Texture Analysis

The glaucoma detection method introduced by Acharya et al. [41] exploits *higher-order spectra* (HOS) features that are combined with texture features.

The proposed HOS features exploit phase and amplitude information of fundus images. Spectral descriptors are obtained from this information and are used as features for glaucoma classification.

The variation of pixel values in an image encodes its texture. For the extraction of texture features, two quantities are analyzed:

- (i) The *gray-level co-occurrence matrix* encodes the number of combinations for different pixel values in an image. Additionally, a difference matrix encodes probabilities that a certain gray-level differences between two pixels occur. This is derived from the co-occurrence matrix.
- (ii) The *run-length matrix*  $P_{\theta}(i, j)$  encodes how often a pixel value  $i$  successively appears  $j$  time for a certain direction given by angle  $\theta$ . From these quantities, texture descriptors are derived as features. For a mathematical definition of the complete feature set, the interested reader is referred to [41].

HOS and texture features are combined as a joint feature set to discriminate healthy and glaucoma subjects. Therefore, SVM, random forests, and naive Bayes classifiers have been investigated showing competitive performance in terms of sensitivity and specificity.

### 9.4.2.2 Wavelet-Based Features

Dua et al. [42] proposed to use the *discrete wavelet transform* (DWT) as a feature extractor in glaucoma detection from fundus images showing the ONH.

The DWT decomposes the input signal, i.e., the fundus image, into spatial and frequency domains at different scalings and is well established in signal and image processing. To identify the most discriminative descriptors for glaucoma detection, this extensive set of features is then reduced by feature ranking and selection. Similar to [41], several classifiers such as random forest, SVM, and naive Bayes have been investigated.

### 9.4.2.3 Eigenimages and Glaucoma Risk Index (GRI)

The concept of appearance-based pattern recognition for glaucoma detection on fundus images was introduced by Bock et al. [6] and is inspired by the *Eigenimages* originally proposed for face recognition [43].

First, input images are preprocessed using ONH centering, illumination correction, and blood vessel inpainting to remove image characteristics not related to glaucoma. Then, three different feature types are extracted from the images: (i) the raw image intensities, (ii) the Fourier coefficients, and (iii) the B-spline coefficients. Each of these feature sets is separately compressed by an unsupervised PCA to condense the major image variations into a compact format. Finally, an SVM classifier hierarchy is employed. In the first stage, each feature vector per feature type is classified by one probabilistic SVM yielding three distinct glaucoma probabilities. In the second stage, these three probabilities are then merged to an intermediate feature vector and used as input for an additional probabilistic SVM to obtain a final probabilistic *glaucoma risk index* (GRI). The processing pipeline for the GRI computation is outlined in Fig. 9.5.

### 9.4.2.4 Independent Component Analysis

A further appearance-based method for glaucoma detection has been proposed by Fink et al. [44]. This method utilizes the *independent component analysis* (ICA) [45] on images captured with a confocal laser ophthalmoscope (Heidelberg retina tomograph (HRT)). In contrast to PCA,

ICA decomposes the signal into statistically independent factors. The entire HRT image is treated as a feature vector and used to derive its ICA decomposition coefficients. The final classification is then achieved by applying a K-nearest neighbor classifier utilizing these coefficients as a feature.

## 9.5 Summary

This section summarizes the performance of the described structural and data-driven approaches. Subsequently, both paradigms are discussed and compared.

### 9.5.1 Performance Comparison

For quantitative evaluation, the following measurements are considered: (i) the accuracy to assess the percentage of correctly classified images, (ii) the sensitivity and specificity to quantify the trade-off between a sensitive glaucoma detection and an unreasonable high false-positive rate, and (iii) the area under the *receiver operating characteristic curve* (AUC) to evaluate for the overall performance. While the AUC measurement is independent from a binary cut-off threshold during classification, the remaining measurements might be adjusted by selecting a different threshold, e.g., optimized for a screening scenario. Table 9.1 summarizes quantitative results as reported in the cited original publications. The numbers are not necessarily gained from the same sample set and may have different distributions of

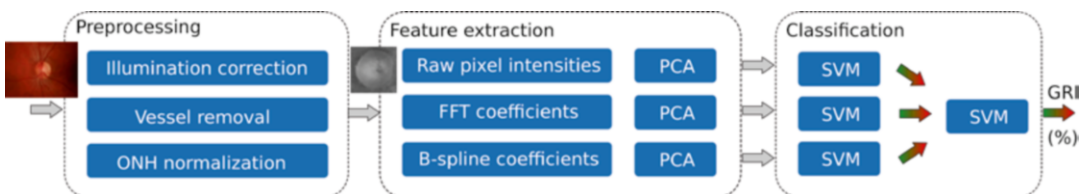


**Fig. 9.5** Glaucoma risk index (GRI): The processing pipeline performs three major steps: (i) preprocessing to eliminate disease independent variations, (ii) data-driven feature extraction based on different feature types and

principal component analysis (PCA), and (iii) two-stage probabilistic classification using support vector machine (SVM) to achieve the final risk index



**Table 9.1** Summary of cited references for data-driven (*D*) and structure-driven (*S*) approaches. Imaging modalities utilized for glaucoma detection are fundus imaging (*FI*), the Heidelberg retina tomograph (*HRT*) for topographic analysis, and optical coherence tomography (*OCT*) for volumetric analysis. A measure is omitted (–) if it is not reported in the original publication

Method	S/D	Modality	Images	Sens. (%)	Spec. (%)	Acc. (%)	AUC (%)
<b>Fundus images (2-D)</b>							
Cheng et al. [25]	S	FI	2,326	–	–	–	82
Superpixels, cup-to-disk ratio (CDR)							
Nayak et al. [9]	S	FI	61	100	80	90	–
CDR, ISNT rule (inferior-superior-nasal-temporal)							
Acharya et al. [41]	D	FI	60	–	–	92	–
Higher-order spectra (HOS), texture							
Dua et al. [42]	D	FI	60	–	–	93	–
Wavelet							
Bock et al. [6]	D	FI	575	73	85	80	88
Eigenimages, principal component analysis (PCA)							
<b>Topographic analysis</b>							
Swindale et al. [11]	S	HRT	200	88	89	89	–
Glaucoma probability score (GPS)							
Twa et al. [32]	S	HRT	275	69	88	80	88
Zernike polynomial							
Fink et al. [44]	D	HRT	120	–	–	91	–
Independent component analysis (ICA)							
<b>Volumetric analysis</b>							
Bizios et al. [38]	S	OCT	152	–	–	–	98
Retinal nerve fiber layer (RNFL) measurements							
Mayer et al. [39, 40]	S/D	OCT	204	90	90	–	94
(RNFL, PCA)							

glaucoma disease, age, sex, or race. If multiple classifiers were evaluated on the same feature set, we report the best performance achieved.

The results indicate that image-based glaucoma detection achieves a notable accuracy and an AUC of at least 80 %, respectively. Considering fundus photography and HRT imaging, both structural and data-driven methods can achieve an accuracy of around 90 %. However, volumetric analysis based on OCT data is characterized by an outstanding AUC of up to 98 %. Thus, neither structural nor data-driven methodology is outperforming the other one, while the volumetric, structure-driven techniques seem to be most discriminative.

### 9.5.2 Structure-Driven vs. Data-Driven Approach

The presented paradigms achieve a comparable glaucoma detection performance within the same imaging modality although they both rely on contrary basic assumptions.

Structure-driven methods depend on a small, but highly discriminative, set of features, neglecting the bigger part of the image data. In general, these are either computed by fitting a parametric model to the image data or segmenting retinal structures. The obtained indicators were manually selected and proved by clinical studies and/or trials. In mass screening, an automated and reliable analysis, e.g., of the CDR, relies on an accurate segmentation of cup and disk. However, since boundaries of these structures are not well defined and highly variable, such an automatism is difficult to achieve in practice.

In data-driven approaches, no manual preselection of the image content is performed, but the entire image data is utilized. The desired compact set of discriminative features required for a reasonable classification is then obtained by a subsequent automatic feature selection and compression. Thus, the data-driven techniques might extract novel features that are not yet captured by structure-driven approaches. A further medical analysis of these data-driven features is promising as it might provide new insights to glaucoma disease and its variations.

## Conclusion

This chapter presents novel trends for glaucoma detection by means of pattern recognition. These techniques employ noninvasive and in vivo imaging of the human retina and can be embedded to computer-aided screening. In the course of this chapter, methods based on fundus photography, topographic HRT imaging, and volumetric analysis using OCT are reviewed. The two major methodologies, i.e., (i) structure- and (ii) data-driven techniques, utilize complementary image information and showed a comparable performance.

Even when first experimental evaluations showed promising results, there are several ways to extend these techniques and to gain new insight to glaucoma disease and its characteristics. Since all presented methods employ a single imaging modality, multimodal techniques are an interesting extension. Therefore, complementary information, e.g., 2-D photometric data obtained from fundus photography augmented by volumetric data acquired by OCT, can be used to extract a multimodal feature set. In addition, features obtained by structural and data-driven methods can be combined to a hybrid classification approach. This might improve automatic glaucoma detection in order to reduce the amount of manually assessed screening patients and may help to reduce the costs of glaucoma screening programs.

**Acknowledgment** The authors gratefully acknowledge funding of the Erlangen Graduate School in Advanced Optical Technologies (SAOT) by the German National Science Foundation (DFG) in the framework of the excellence initiative.

## References

1. Quigley HA, Broman AT. The number of people with glaucoma worldwide in 2010 and 2020. *Br J Ophthalmol.* 2006;90(3):262–7.
2. Glaucoma Research Foundation. Glaucoma facts and stats. 2013. Available from: <http://www.glaucoma.org>.
3. European Glaucoma Society, editor. Terminology and guidelines for glaucoma. 2nd ed. Savona: Editrice Dogma; 2003.

4. Bonomi L, Marchini G, Marraffa M, Bernardi P, De Franco I, Perfetti S, et al. Prevalence of glaucoma and intraocular pressure distribution in a defined population: the Egna-Neumarkt Study. *Ophthalmology*. 1998;105(2):209–15.
5. Momont AC, Mills RP. Glaucoma screening: current perspectives and future directions. *Semin Ophthalmol*. 2013;28(3):185–90.
6. Bock R, Meier J, Nyil LG, Hornegger J, Michelson G. Glaucoma risk index: automated glaucoma detection from color fundus images. *Med Image Anal*. 2010;14(3):471–81.
7. Patton N, Aslam TM, MacGillivray T, Deary IJ, Dhillon B, Eikelboom RH, et al. Retinal image analysis: concepts, applications and potential. *Prog Retin Eye Res*. 2006;25(1):99–127.
8. Budai A, Odstrčilik J. High resolution fundus image database. 2013. Available from: <http://www5.cs.fau.de/research/data/fundus-images>.
9. Nayak J, Acharya UR, Bhat PS, Shetty N, Lim TC. Automated diagnosis of glaucoma using digital fundus images. *J Med Syst*. 2008;33(5):337–46.
10. Kruse F, Burk R, Völcker H, Zinser G, Harbarth U. Reproducibility of topographic measurements of the optic nerve head with laser tomographic scanning. *Ophthalmology*. 1989;96(9):1320–4.
11. Swindale NV, Stjepanovic G, Chin A, Mikelberg FS. Automated analysis of normal and glaucomatous optic nerve head topography images. *Invest Ophthalmol Vis Sci*. 2000;41(7):1730–42.
12. Huang D, Swanson EA, Lin CP, Schuman JS, Stinson WG, Chang W, et al. Optical coherence tomography. *Science*. 1991;254(5035):1178–81.
13. Huang ML, Chen HY. Development and comparison of automated classifiers for glaucoma diagnosis using Stratus optical coherence tomography. *Invest Ophthalmol Vis Sci*. 2005;46(11):4121–9.
14. Burgansky-Eliash Z, Wollstein G, Chu T, Ramsey JD, Glymour C, Noecker RJ, et al. Optical coherence tomography machine learning classifiers for glaucoma detection: a preliminary study. *Invest Ophthalmol Vis Sci*. 2005;46(11):4147–52.
15. Bishop CM. *Pattern recognition and machine learning (information science and statistics)*. Secaucus: Springer-Verlag New York, Inc.; 2006.
16. Niemeijer M, Abramoff MD, Van Ginneken B. Image structure clustering for image quality verification of color retina images in diabetic retinopathy screening. *Med Image Anal*. 2006;10(6):888–98.
17. Köhler T, Budai A, Kraus MF, Odstrčilik J, Michelson G, Hornegger J. Automatic no-reference quality assessment for retinal fundus images using vessel segmentation. In: *IEEE 26th international symposium on Computer-Based Medical Systems (CBMS)*. Porto; 2013. p. 95–100.
18. Paulus J, Meier J, Bock R, Hornegger J, Michelson G. Automated quality assessment of retinal fundus photos. *Int J Comput Assist Radiol Surg*. 2010;5(6):557–64.
19. Abramoff MD, Garvin MK, Sonka M. Retinal imaging and image analysis. *IEEE Reviews in Biomedical Engineering*. 2010;3:169–208.
20. Kubecka L, Jan J, Kolar R. Retrospective illumination correction of retinal images. *Int J Biomed Imaging*. 2010;2010:1–10.
21. Köhler T, Hornegger J, Mayer M, Michelson G. Quality-guided denoising for low-cost fundus imaging. In: *Bildverarbeitung für die Medizin 2012*. Berlin-Heidelberg: Springer; 2012. p. 292–7.
22. Meier J, Bock R, Michelson G, Nyl LG, Hornegger J. Effects of preprocessing eye fundus images on appearance based glaucoma classification. In: *12th international conference on Computer Analysis of Images and Patterns, CAIP. Lecture Notes in Computer Science (LNCS) 4673*, vol. 4673/2007. Vienna; 2007. p. 165–73.
23. Joshi GD, Sivaswamy J, Krishnadas S. Optic disk and cup segmentation from monocular color retinal images for glaucoma assessment. *IEEE Trans Med Imaging*. 2011;30(6):1192–205.
24. Yin F, Liu J, Wong DWK, Tan NM, Cheung C, Baskaran M, et al. Automated segmentation of optic disc and optic cup in fundus images for glaucoma diagnosis. In: *2012 25th IEEE international symposium on Computer-Based Medical Systems (CBMS)*. IEEE Rome; 2012. p. 1–6.
25. Cheng J, Liu J, Xu Y, Yin F, Wong DWK, Tan NM, et al. Superpixel classification based optic disc and optic cup segmentation for glaucoma screening. *IEEE Trans Med Imaging*. 2013;32(6):1019–32.
26. Michelson G, Wärtiges S, Hornegger J, Lausen B. The papilla as screening parameter for early diagnosis of glaucoma. *Dtsch Arztebl Int*. 2008;105(34–35):583–9.
27. Sharma P, Sample PA, Zangwill LM, Schuman JS. Diagnostic tools for glaucoma detection and management. *Surv Ophthalmol*. 2008;53 Suppl 1:S17–32.
28. Horn FK, Mardin CY, Laemmer R, Baleanu D, Juenemann AM, Kruse FE, et al. Correlation between local glaucomatous visual field defects and loss of nerve fiber layer thickness measured with polarimetry and spectral domain OCT. *Invest Ophthalmol Vis Sci*. 2009;50(5):1971–7.
29. Muramatsu C, Nakagawa T, Sawada A, Hatanaka Y, Yamamoto T, Fujita H. Automated determination of cup-to-disc ratio for classification of glaucomatous and normal eyes on stereo retinal fundus images. *J Biomed Opt*. 2011;16(9):096009.
30. Hancox ODMD. Optic disc size, an important consideration in the glaucoma evaluation. *Clin Eye Vision Care*. 1999;11(2):59–62.
31. Fayers T, Strouthidis NG, Garway-Heath DF. Monitoring glaucomatous progression using a novel Heidelberg Retina Tomograph event analysis. *Ophthalmology*. 2007;114(11):1973–80.
32. Twa MD, Parthasarathy S, Johnson CA, Bullimore MA. Morphometric analysis and classification of glaucomatous optic neuropathy using radial polynomials. *J Glaucoma*. 2012;21(5):302–12.
33. Mayer M, Borsdorf A, Wagner M, Hornegger J, Mardin CY, Tornow RP. Wavelet denoising of multi-frame optical coherence tomography data. *Biomed Optics Expr*. 2012;3(3):572–89.

34. Salinas HM, Fernandez DC. Comparison of PDE-based nonlinear diffusion approaches for image enhancement and denoising in optical coherence tomography. *IEEE Trans Med Imaging*. 2007; 26(6):761–71.
35. Ozcan A, Bilenca A, Desjardins AE, Bouma BE, Tearney GJ. Speckle reduction in optical coherence tomography images using digital filtering. *J Opt Soc Am A Opt Image Sci Vis*. 2007;24(7):1901–10.
36. Kraus M, Potsaid B, Mayer M, Bock R, Baumann B, Liu JJ, et al. Motion correction in optical coherence tomography volumes on a per A-scan basis using orthogonal scan patterns. *Biomed Optics Expr*. 2012;3(6):1182–99.
37. Pachiyappan A, Das UN, Murthy TV, Tatavarti R. Automated diagnosis of diabetic retinopathy and glaucoma using fundus and OCT images. *Lipids Health Dis*. 2012;11:73.
38. Bizios D, Heijl A, Hougaard JL, Bengtsson B. Machine learning classifiers for glaucoma diagnosis based on classification of retinal nerve fibre layer thickness parameters measured by Stratus OCT. *Acta Ophthalmol*. 2010;88(1):44–52.
39. Mayer MA, Hornegger J, Mardin CY, Kruse FE, P TR. Automated glaucoma classification using nerve fiber layer segmentations on circular spectral domain OCT b-scans. The Association for Research in Vision and Ophthalmology, Inc. (ARVO) (Annual Meeting), E-Abstract. 2009.
40. Mayer MA, Hornegger J, Mardin CY, Tornow RP. Retinal nerve fiber layer segmentation on FD-OCT scans of normal subjects and glaucoma patients. *Biomed Optics Expr*. 2010;1(5):1358.
41. Acharya UR, Dua S, Du X, Sree SV, Chua CK. Automated diagnosis of glaucoma using texture and higher order spectra features. *IEEE Trans Inf Technol Biomed*. 2011;15(3):449–55.
42. Dua S, Acharya UR, Chowriappa P, Sree SV. Wavelet-based energy features for glaucomatous image classification. *IEEE Trans Inf Technol Biomed*. 2012;16(1):80–7.
43. Turk M, Pentland A. Eigenfaces for recognition. *J Cogn Neurosci*. 1991;3(1):71–86.
44. Fink F, Worle K, Gruber P, Tome A, Gorriz-Saez J, Puntonet C, et al. ICA analysis of retina images for glaucoma classification. In: *Engineering in Medicine and Biology Society, 2008. EMBS 2008. 30th annual international conference of the IEEE*. IEEE Vancouver; 2008. p. 4664–7.
45. Hyvärinen A, Oja E. Independent component analysis: algorithms and applications. *Neural Netw*. 2000;13(4):411–30.